REPORT DOCUMENTATION PAGE

Form Approved
OMB No. 0704-0188

1. REPORT DATE *(DD-MM-YYYY)*	2. REPORT TYPE	3. DATES COVERED *(From - To)*
	Technical Paper	

4. TITLE AND SUBTITLE

5a. CONTRACT NUMBER

5b. GRANT NUMBER

5c. PROGRAM ELEMENT NUMBER
62500F

6. AUTHOR(S)

5d. PROJECT NUMBER
2308

5e. TASK NUMBER
M4S7

5f. WORK UNIT NUMBER
345382

7. PERFORMING ORGANIZATION NAME(S) AND ADDRESS(ES)

8. PERFORMING ORGANIZATION REPORT

9. SPONSORING / MONITORING AGENCY NAME(S) AND ADDRESS(ES)

Air Force Research Laboratory (AFMC)
AFRL/PRS
5 Pollux Drive.
Edwards AFB CA 93524-7048

10. SPONSOR/MONITOR'S ACRONYM(S)

11. SPONSOR/MONITOR'S NUMBER(S)

12. DISTRIBUTION / AVAILABILITY STATEMENT

Approved for public release; distribution unlimited.

13. SUPPLEMENTARY NOTES

See attached 13 papers, all with the information on this page.

14. ABSTRACT

15. SUBJECT TERMS

16. SECURITY CLASSIFICATION OF:			17. LIMITATION OF ABSTRACT	18. NUMBER OF PAGES	19a. NAME OF RESPONSIBLE PERSON
a. REPORT	b. ABSTRACT	c. THIS PAGE			Kenette Gfeller
Unclassified	Unclassified	Unclassified	A		19b. TELEPHONE NUMBER *(include area code)* (661) 275-5016

AIAA-94-3302

Interior Spectroscopic Investigation of the Propellant Energy Modes in an Arcjet Nozzle

W. Hargus and M. Micci
Pennsylvania State University
University Park, PA

R. Spores
OL-AC Phillips Laboratory
Edwards Air Force Base, CA

PENNSTATE

1855

PHILLIPS LABORATORY

30th AIAA/ASME/SAE/ASEE Joint Propulsion Conference
June 27-29, 1994 / Indianapolis, IN

Interior Spectroscopic Investigation of the Propellant Energy Modes in an Arcjet Nozzle

William A. Hargus, Jr.*, Michael M. Micci**

The Pennsylvania State University

Dept. of Aerospace Engineering, University Park, PA 16802

Ronald A. Spores†

OL-AC Phillips Laboratory, Edwards AFB, CA 93524

Abstract

Internal emission spectroscopy measurements were performed in the nozzle expansion region of a 26 kW class ammonia arcjet. A series of three optical access ports (0.020 inch diameter) were equally spaced along the center line of the expansion nozzle. Atomic and ionic excitation temperatures of H and NII were determined through the use of Boltzmann plots. Electron density measurements were also taken based upon Stark broadening of the hydrogen beta Balmer transition. It is believed that a change in the mechanism governing the electron density occurred just downstream of the constrictor between the first two access ports lending evidence that arc attachment is occurring in this region. Although the trends for excitation temperatures and electron density were similar to those previously observed in 1 kW arcjets, the temperature values were found to be significantly less. In addition, vibrational and rotational temperatures of NH were measured and appeared to be frozen throughout the expansion nozzle.

Introduction

Arcjets are expected to play an ever increasing role in satellite propulsion needs, primarily stationkeeping and on-orbit maneuvering in the near future. While the technology is considered viable enough to be deployed on a Telstar IV communications satellite for stationkeeping [1], arcjets are far from a mature technology. Beyond stationkeeping, one of the next steps for electric propulsion will be orbit transfer. With the upcoming ESEX flight test of a high power arcjet in late 1995 [2], high power arcjet technology is being advanced to fill this niche.

Unfortunately, current high power arcjet designs suffer from low efficiencies, converting only 30% of the input electrical power to thrust for the storable propellant ammonia. These efficiency levels are considered marginal for accomplishing orbit transfer missions in an acceptable time frame for the Air Force. Therefore, a greater understanding of the physics within the arcjet is required so that significant improvements in future high power arcjet performance maybe realized. While extensive work has been performed in the plume region, it is strongly believed that the investigation must shift to the interior region of the arcjet in order to make further progress. Toward this goal, a research program was conducted to determine the propellant energy characteristics within the nozzle of an arcjet using emission spectroscopy.

To increase the overall efficiency of an arcjet, it is important to understand the major energy losses, of which frozen flow is believed to be dominant. Frozen flow losses of arcjet plasma species include: unrecovered dissociation, electronic excited states, ionization, and rotational-vibrational energy trapped within their respective modes. The purpose of this investigation is to gain a better understanding of these loss mechanisms within the arcjet expansion region. Information obtained from this research about the energy distribution in an arcjet is beneficial for both designing next-generation thrusters and as an essential database for improving computational codes. Neutral excitation, ionic excitation, vibrational, and rotational temperatures, along with electron density, were determined using a variety of spectroscopic techniques.

Computational models have predicted the plasma properties within arcjets; however, only a few researchers have performed diagnostics within arcjet thrusters. Several papers have been presented by Tahara, et al, on water cooled arcjets with internal optical access provided by quartz windows [3, 4]. However, the use of active cooling, necessary for the survival of the windows, renders these studies questionable for comparison with models of radiatively cooled operational thrusters. Other studies have examined the interior plasmas of

low and medium power arcjets by emission spectroscopy: axial measurements were taken by Storms and Cappelli [5], angled into the arcjet nozzle by Ruyten, et al [6], and measurements through small optical access ports into the side of the arcjet were accomplished by Zube and Myers [7] and later by Zube and Auweter-Kurtz [8]. These studies were performed on low and medium power arcjets and apply to the present generation of operational arcjets. However, until now no study has directly examined the plasma within the nozzle expansion of the next generation of high power arcjets to be used for orbit raising and orbit transfer missions.

Experimental Apparatus

Arcjet

The arcjet used for this research program was the USAF 26 kW class laboratory thruster [9]; the basic arcjet configuration is shown in Figure 1. The area ratio of the nozzle is 100 with a constrictor length and diameter of 0.1 inches, a nozzle half angle of 19°, and a expansion nozzle length of 1.307 inches. The arcjet was operated on 250 mg/sec of ammonia at a power level of only 17.7 kW (151 A, 117 V) to minimize erosion of the optically accessible nozzle. During data acquisition, the background pressure was 200 mTorr.

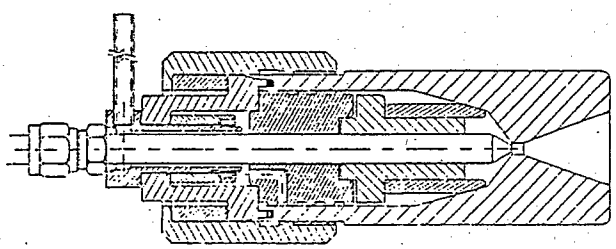

Figure 1. Test Thruster

Optical Access Ports

The optical access into the nozzle was provided via 3 small holes positioned in line through both sides of the nozzle to minimize internal reflections and radiation from the far nozzle wall; the locations of these optical access ports is shown in Figure 2. Similar work performed on a low power arcjet operating on simulated hydrazine by Zube and Myers [7] showed that internal reflections from the nozzle adversely affected data acquisition. By placing their optical access holes through the arcjet constrictor region, Zube and Auweter-Kurtz [8] showed that reflections were insignificant when compared to the total signal. From the interior wall of the arcjet nozzle, a 0.020 inch diameter optical access passage was electron deposition machined (EDM) for the first 0.100 inches; at that point, the port was expanded to 0.080 inches until the outer edge of the anode/nozzle. The most upstream optical access port was placed just downstream of the constrictor (by 0.100 inches) while the remaining two were placed equidistantly between the first port and the nozzle exit. The ratios of the access hole area to the local nozzle expansion area compared similarly, or smaller, to those of reference 7 where it was determined that the optical access ports did not affect the performance of the arcjet within the resolution of their thrust stand (<2%). Thrust measurements, with the holes both open and plugged, are the best method for determining whether the technique is intrusive. Unfortunately, thrust stand measurements have not been taken as of this writing.

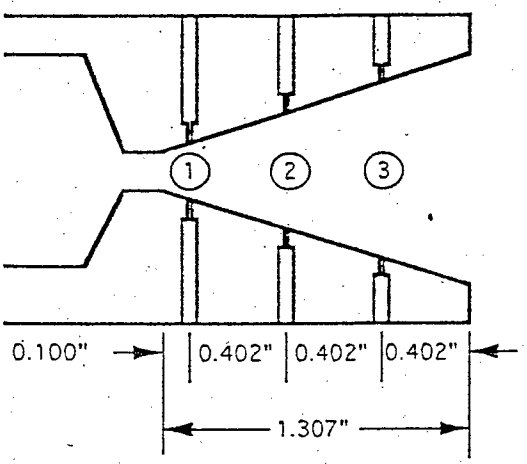

Figure 2. Optical Access Placement

Experimental Setup

This project was conducted in vacuum chamber 2 of the USAF Electric Propulsion Laboratory of the Phillips Laboratory at Edwards AFB, California. As shown in Figure 3, a cooling system was installed to duct the arcjet exhaust and reduce heat transfer to the vacuum chamber. In addition, an arcjet mount was constructed to minimize thermal conduction to the positioning system. The mount was placed on a Daedel translation table with 12 x 12 inch range of horizontal travel. Vertical positioning was provided by a rail table with a total travel of 6 inches. Both positioners were capable of 0.001 inch repeatability and straight line accuracies of 0.0005 in/in to provide proper alignment of the spectroscopy collection system with the optical access holes. Propellant flow was regulated by an MKS 1542 mass flow controller configured for ammonia while background pressures were measured via an MKS Baratron 122AB capacitance manometer.

An emission spectroscopy system was developed specifically for internal arcjet optical diagnostics. Figure 4 shows the optical train used to collect the emission signal from the arcjet interior through the optical access ports. After the signal is collected, it is focused onto the entrance slit of a Czerny-Turner 0.5 m Acton Research SpectraPro-500 spectrometer. The spectrometer contained a turret with three holographically blazed gratings of 2400, 1200, and 600 groove/mm. At a wavelength of 435.8 nm and with a 1200 groove/mm grating, the system had a resolution of 0.05 nm in the first order. A Princeton Instruments thermo-electrically cooled CCD detector with a UV scintillator was used to obtain the resultant spectra. A relative intensity calibration of the spectroscopy system was performed by focusing on the filament of a 6.5 A quartz halogen tungsten calibrated standard

of spectral irradiance with a calibration traceable to the National Institute of Standards and Technology.

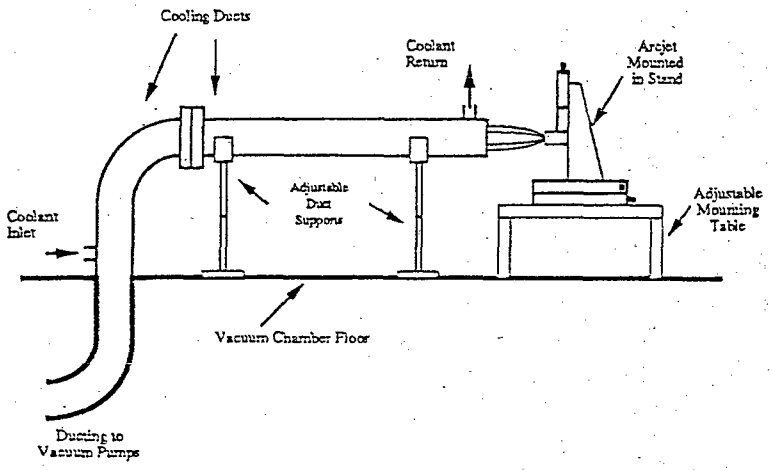

Figure 3. Mount and Cooling System

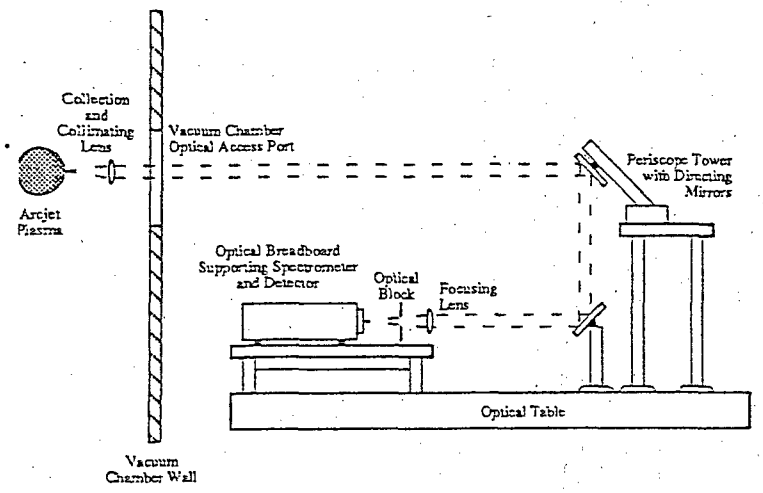

Figure 4. Optical Train

Spectroscopic Techniques

Excitation and Electron Temperatures

For the experiments discussed here, the standard Boltzmann plot technique was employed to obtain excited state temperatures. If the spectral resolution allowed, data from 5-10 transition lines were used with the following equation,

$$\ln\left[\frac{I_{ij}\lambda_{ij}}{cA_{ij}g_i}\right] = -\frac{E_i}{kT} + \ln\left(\frac{hn}{2\pi Z}\right) \qquad (1)$$

where I_{ij} is the intensity of the transition from level i to level j, T is the temperature, λ_{ij} is the wavelength of the transition, A_{ij} is the atomic transition probability, E_i is the energy of the upper level, k is the Boltzmann constant, h is the Planck constant, n is the species density, Z is the electronic partition function, and c is the speed of light in a vacuum. The temperature can be then determined from the slope of the line of the right hand side of the equation plotted versus the energy E_i of each upper level of the transition. Since only the slope of the line is of interest, the values inside the logarithmic terms need only be known relatively to determine temperature. In arcjet plasmas where partial local thermodynamic equilibrium (PLTE) conditions usually exist, the lower energy levels are likely to be underpopulated and the resulting transitions from these levels are not in equilibrium with one another. Higher energy levels are more likely to be in collisional, and thus thermal, equilibrium with the electrons of the plasma [10, 11]. By only using these higher energy levels in the Boltzmann plot, it is believed that a more representative temperature of the arcjet plasma can be obtained.

Vibrational and Rotational Temperatures

Since different energy modes are available within the plasma, several distinct and non-equilibrated temperatures can be thought to exist. Due to sufficient molecular recombination or the lack of dissociation, polyatomic species will exist in the cooler plasma regions of an arcjet nozzle. Two modes of energy deposition, the vibrational and rotational oscillatory modes, can be found for polyatomic species through the use of emission spectroscopy. For this work, the vibrational and rotational temperatures of NH were determined. The NH vibrational-rotational transitions represent the second most intense spectral features after the hydrogen Balmer series and are in an easily accessed portion of the spectrum.

Vibrational temperatures of NH were determined assuming local thermodynamic equilibrium (LTE) and using the integrated intensity ratio of two vibrational-rotational bands. A Boltzmann type plot of a number of bands would have resulted in a more precise measurement and allowed for a quantification of the equilibrium of the vibrational energy levels. However, NH presented only two vibrational transitions that were of sufficient intensity. The transitions used to determine the NH vibrational temperature were the Q branches of the $v''=0 \rightarrow v'=0$ and $v''=1 \rightarrow v'=1$ vibrational transitions of the $A^3\Pi \rightarrow X^3\Sigma^-$ electronic transition. These two transitions have band heads at 336.1 and 337.3 nm, respectively [12]. Unfortunately, the $v''=2 \rightarrow v'=2$ band was not clearly observable; however, even under ideal conditions, it is several orders of magnitude less intense. It is believed that for this plasma, NH is undergoing a lowering of the ionization potential that does not allow the third vibrational transition to occur [13]. Required spectral constants were taken from Lents [14]. Vibrational

temperatures were calculated from the intensity ratio of two molecular bands using the following equation,

$$T_{Vib} = \frac{G_1 - G_2}{kLn\left[\frac{I_2\lambda_2^4 f_1}{I_1\lambda_1^4 f_2}\right]} \qquad (2)$$

where G is the energy of the specified vibrational level and f is the absorption oscillator strength [15]. This method requires that the spectral bands be free of overlap so that the total intensities of the bands can be determined unambiguously. The absolute uncertainty of the vibrational temperatures found from Equation 2 is limited by the uncertainty in the oscillator strength values to 25% [7, 15].

The rotational spectra of NH contain a complex band structure that also did not allow a Boltzmann plot analysis to be performed from the emission data. The complex spectral structure is due to the coupling of the rotational angular momentum to the spin angular momentum of the unpaired electrons of the $^3\Pi$ upper and $^3\Sigma^-$ lower states of NH, each of the rotational levels is caused to split into three sub-levels of slightly different energy with upper rotational states exhibiting larger splitting. For the individual rotational energy levels, the transitions in the R and P branches were multiplets of three lines having identical angular momentum about the nuclear axis, but different spins [15, 16].

The rotational temperature of NH was determined by direct comparison of observed spectra with an analytical model. Due to the dense structure and complexity of rotational spectral bands, the preferred method for obtaining rotational temperatures is by modeling the rotational spectra and iteratively varying the rotational temperature until a match is achieved with the experimentally acquired spectra. Previous studies of internal arcjet plasmas have utilized N_2 and N_2^+ vibrational-rotational bands where individual rotational transitions exhibit strong overlap and are not individually distinguished [4, 7]. The finite resolution of the spectrometer is not an issue in these measurements since the instrument function can be convolved with modeled results to simulate the limited resolution of the detection system. A computer code developed by Welle was used to simulate the $v''=0 \rightarrow v'=0$ P branch of the NH $A^3\Pi \rightarrow X^3\Sigma^-$ transition [17]. For measurements at the maximum available dispersion (2400 grooves/mm) where the triplet structure of the rotational transitions of NH were not completely resolved, an instrument function with a full width at half maximum (FWHM) of 4 wave numbers was found to match the spectrometer resolution. The simulated rotational spectra, at 250 K intervals, were compared to experimental data until the best match was made.

Electron Densities

Electron densities were determined from the full width at half maximum (FWHM) of the Balmer beta line using the method outlined by Griem [11]. The electron density and Stark component of the FWHM of a broadened line are almost exactly proportional to the $^2/_3$rd power and can be written as,

$$n_e = C(n_e, T_e)\Delta\lambda_s^{2/3} \qquad (3)$$

where $C(n_e, T_e)$ is a function weakly dependent on electron density and temperature and $\Delta\lambda_s$ is the Stark component of the FWHM of the line. Equation 3 is valid only as long the electrons and singly charged ions are the only charged particles in the plasma. To use Equation 3, $C(n_e, T_e)$ must be interpolated from the tabulated values given by Griem. Then, several iterations are performed until the electron density and previously determined electron temperature are consistent. The electron densities are believed to have an experimental uncertainty of approximately 20%.

Experimental Results

Interior Plasma Characteristics

Initial measurements through the optical access ports showed that diagnostics well suited to the plume were not always effective within the arcjet nozzle. While conditions in the furthest downstream optical port approached those of the plume, conditions at port 1 differed significantly. Spectral lines not visible in the plume, such as ionized atomic nitrogen (NII), were readily apparent in hole 1. Increased spectral broadening for the upstream holes, due to the high electron densities which resulted in higher Stark broadening, was especially severe in the hydrogen Balmer series. For this reason, courser gratings (1200 versus 2400 grooves/mm) were required to reduce the total dispersion of the spectrometer in order to capture the entire line shape of the Balmer series on the CCD detector.

Hydrogen and several nitrogen spectra (N_2, NI, NII) were initially examined for use in determining temperature data. Several other species were also apparent during the initial survey of the internal plasma. An attempt was made to utilize the N_2 bands at 380.4 and 375.4 nm to determine a nitrogen vibrational temperature. Unfortunately, overlap of the two bands did not allow for a vibrational temperature to be determined. Several other molecular bands were also observed, but proved too weak to be of diagnostic use. Molecular hydrogen spectra were visible, but exhibited the extremely open bands that generally make it a poor diagnostic tool. Both NH_2 and NH_2^+ were also seen during testing, but produced very weak bands that were near the UV limit of the detector and spectrometer. An extremely weak set of bands for NH_3 was visible and several weak bands of ionized molecular nitrogen (N_2^+) were observed but not used.

Excitation Temperature Measurements

Boltzmann plots were used to determine excitation temperatures for two species: H and NII. Since the energy levels of the upper excited states employed in this analysis are close to the energy needed for ionization, the free electrons can be assumed to have essentially the same temperature as the uppermost excited states [11].

Although Tahara, et al, and Zube and Myers both used NI spectra to determine excitation temperatures (Tahara by use of Boltzmann plots and Zube and Myers by a ratio of two line intensities), the NI line strengths were found to be too weak to resolve in this study [4, 7]. The reason for this is not fully understood; however, both previous studies used N_2 as a fraction of their propellant. Tahara used approximately 98% nitrogen (~2% hydrogen) as his propellant while Zube and Myers used a nitrogen/hydrogen mixture to simulate hydrazine for their tests. Therefore, a likely explanation is that there are differences in the propellant chemistry that do not allow sufficient quantities of atomic nitrogen to exist in the plasma when ammonia is used as opposed to N_2. Unfortunately, insufficient data of the chemical kinetics within the nozzle were available to determine the actual mechanisms.

Figure 5, which shows a Boltzmann plot generated for NII, gives the excitation temperature of NII at port 1 to be 22,000 K. A total of seven transitions were used to determine this NII excitation temperature Unlike, the hydrogen Balmer series, the NII spectra were not significantly broadened. However, the intensity of the NII spectra were seen to rapidly diminish in the downstream direction. So while the spectra were sufficiently intense to allow the generation of Boltzmann plots for the first hole, the line strengths of the spectra from holes 2 and 3 were insufficient to produce a meaningful measurement.

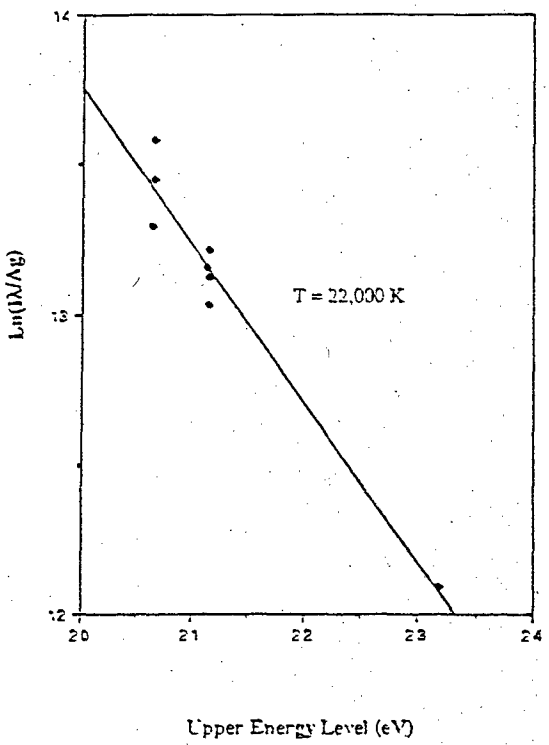

Figure 5. NII Boltzmann Plot at Port 1

The hydrogen Balmer series, which is in the visible and near UV region of the spectrum, is easily accessible for spectroscopic analysis. Unfortunately, the transitions are extremely sensitive to Stark broadening which presented difficulties, especially in port 1. Upper transitions were found to be excessively broadened and indistinguishable from the background at hole 1 and thus Boltzmann plots with more than 4 transitions were only possible from holes 2, 3, and at the exit plane. A further difficulty was that lines from NII overlapped the higher members of the Balmer series making transition intensity determinations difficult or impossible. For hole 1, only the first four Balmer lines were observed before Stark broadening became too severe. After discarding the alpha transition, the remaining three lines were plotted in a Boltzmann plot to determine a hydrogen excitation temperature of 8,500 K. Boltzmann plots of the second and third ports were more readily obtained and the excitation temperatures were found to be 4,800 and 3,400 K, respectively, after discarding both the alpha and beta transitions. Note that the discarded transitions were determined to be underpopulated from the Boltzmann plots and were consequently not used for determining the best fit slope. The discarding of only the lowest transition at port 1 is felt to be justified due to the high electron density within the nozzle at points further upstream allowing for higher electron collisional rates which result in PLTE validity at lower energy levels [11].

In addition to access hole observations, some measurements were made at the exit plane. The first 8 transitions of the hydrogen Balmer series were observed at the exit plane before N_2 bands obscured higher transitions. From these measurements, a Boltzmann plot temperature of 4,800 K was found after discarding the first three underpopulated transitions. The reason for this higher temperature at the exit plane than port 3 is not presently understood.

The difference between the NII and hydrogen excitation temperatures is thought to be a result of the nonuniform flow within the arcjet [18]. The NII ion is much more likely to be concentrated in the hot core flow of the arcjet, where the arc exerts a direct influence on the propellant. On the other hand, hydrogen is believed to be more widely distributed in the expansion process. Therefore, the excitation temperatures of NII and hydrogen represent the electron temperatures of the hot inner core flow and the average across the nozzle diameter, respectively.

As shown in Figure 6, the hydrogen excitation temperature drops quickly in the upstream high density portion of the expansion. Downstream, where the propellant density is lower, the temperature falls off at a slower rate. Expansion of the propellant causes both the temperature and density to drop; the decreasing density reduces the collisional rates significantly, causing the flow to freeze. If equilibrium existed throughout the nozzle, the downstream temperatures would have been lower as energy was redistributed to other modes. Unfortunately, with the frozen flow within the arcjet nozzle, the thermal energy modes of the hot propellant can not be converted to kinetic energy (thrust), and the high temperatures of the exiting propellant represent a significant loss mechanism of the arcjet thruster.

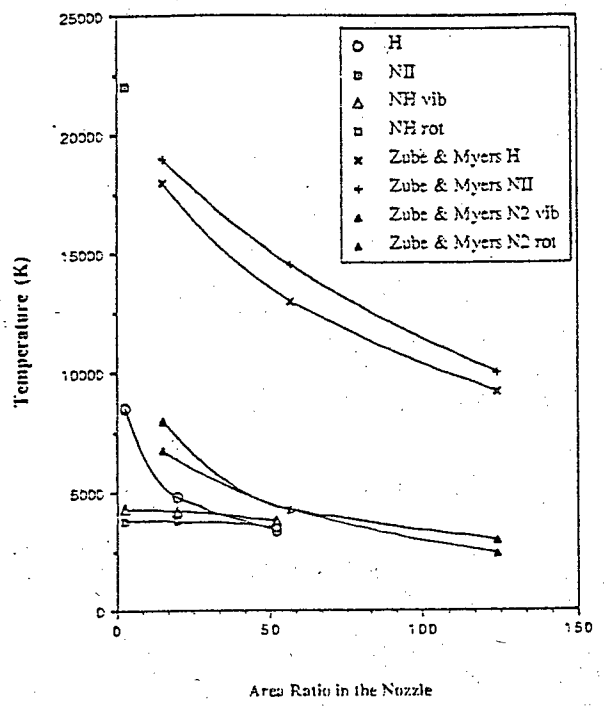

Figure 6. Temperatures Within Nozzle

Although the trends match in the expansion nozzle, the values are quite different when compared to the excitation temperatures found by Zube and Myers [7]. They also showed that the excitation temperatures for the different species within the arcjet (NI, NII, H) appeared to be equilibrated, but this was not evidenced in this work. Since Zube and Myers used only the Balmer alpha and beta transitions in their hydrogen excitation temperature analysis, it may also be implied that their hydrogen temperatures could be higher than the actual electron temperatures due to the effect of underpopulation of the lower two Balmer transitions.

Vibrational and Rotational Temperatures

Spectra from the NH molecule was observed at all access holes and the exit plane providing a strong signal that was distinct from any overlapping spectra. Figure 7 shows the $\nu''=0 \rightarrow \nu'=0$ and $\nu''=1 \rightarrow \nu'=1$ Q branches used to determine the vibrational temperature in port 3 while both the $\nu''=0 \rightarrow \nu'=0$ P branch model and experimental spectra used to determine the rotational temperature are shown in Figure 8. Upon removal of the plasma continuum radiation from the raw spectral data, the vibrational and rotational temperatures were obtained. The vibrational temperatures determined from Equation 2 were found to be 4300, 4200, 3750, and 4600 K for holes 1, 2, 3, and at the exit plane, respectively. Rotational temperatures were 3750, 3750, and 3500 K for holes 1, 2, and 3, respectively.

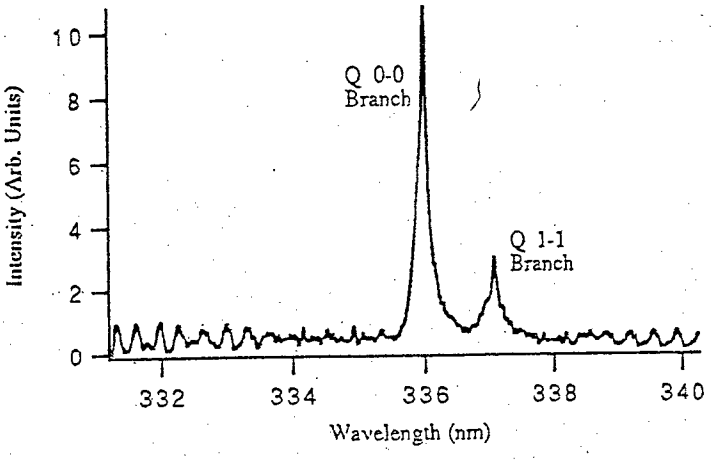

Figure 7. Vibrational NH Spectra

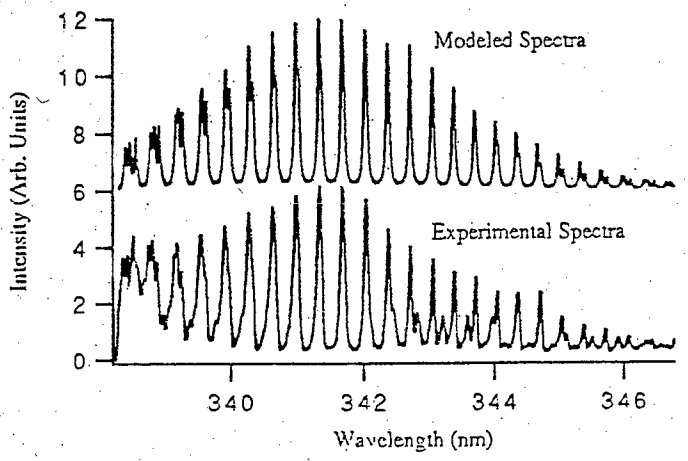

Figure 8. Rotational NH Spectra

The low values of the NH vibrational and rotational temperatures, when compared to the NII excitation temperature, are not only due to differing degrees of excitation within the energy modes of the plasma, but are primarily an artifact of temperature and density nonuniformities within the arcjet [18]. NII, and to a lesser extent hydrogen, are concentrated in the hot, inner core flow of the arcjet. Polyatomic species such as NH cannot survive in the core flow and will only exist along the cooler periphery of the nozzle boundary layer. Therefore, the excitation temperatures are more representative of the core flow in the center of the nozzle expansion while the NH molecular temperatures are more representative of the cooler portions of the flow along the nozzle wall. Density nonuniformities within the arcjet plasma, across the nozzle, biases the resulting spectral signal. In this way, the integrated line of sight measurement taken through the access ports gives spatial bias within the nozzle.

From the near constant values of the vibrational and rotational temperatures within the nozzle, it is assumed that the two molecular energy modes are frozen throughout the expansion. Relaxation rates of the vibrational and rotational modes are implied to be longer than the particle residence times and longer than the de-excitation rates [19]. During previous testing in the plume, vibrational temperatures in the neighborhood of 2,400 K were measured 5 mm from the exit plane.

Only two transitions were used to determine the NH vibrational temperature. This measurement is prone to error if a non-Boltzmann population distribution exists within the relevant vibrational levels. Had more than two vibrational bands been available for analysis, an indication of the equilibrium existing within the vibrational levels could have been made. Counterintuitively, measurements at the exit plane determined a higher vibrational temperature (4,600 K) than that seen at any location within the arcjet. Although there is the possibility that additional heating occurs downstream of the nozzle due to the formation of an expansion shock in the under expanded arcjet flow, this heating mechanism is not considered significant. More likely, the vibrational temperatures must be considered unreliable due to the effect of nonequilibrium populations in the vibrational levels of NH.

While the vibrational temperatures of NH should be viewed with some doubt, the rotational temperatures appear to be more accurate, even though they appear to be in equilibrium with the suspect vibrational temperatures. Some non-Boltzmann behavior among the rotational levels was evident in the band outline of the P branch of the $v''=0 \rightarrow v'=0$ transition, but the degree of non-equilibrium was not severe. Much of the non-Boltzmann shape of the band structure can be attributed to overlap from non-simulated vibrational-rotational transitions, especially the very weak band of the Q branch $v''=2 \rightarrow v'=2$ vibrational band in the neighborhood of 388.3 nm. Therefore, apparent nonequilibrium effect was not felt to be significant and there is a strong degree of confidence in the measured rotational temperatures.

The near constant behavior of the vibrational and rotational temperatures of NH is not easily explained. It is possible that the subtraction of the estimated plasma continuum radiation adversely affected the vibrational temperature determination. Yet, analysis of the raw data strongly indicated that a subtraction was warranted. The rotational temperature determination especially appeared to confirm the procedure. If the vibrational and rotational temperature determinations are accurate, the modes would appear to be frozen and the relaxation rates less than the particle residence times. In addition, the NH present in the flow would be in the thick, yet cooler boundary layer within the arcjet where the gas temperatures are possibly moderated by the temperature of the adjacent inner wall of the nozzle.

NH appears to be a dissociation product of the ammonia propellant as it is heated, rather than a product of a recombination process within the nozzle. The main location of NH formation is believed to be in the constrictor and plenum regions where the majority of the propellant heating occurs. NH formation from recombination in the nozzle boundary layers of dissociation products that diffused from the central core flow is considered secondary due to the weak spectral signal of NI throughout the nozzle.

Although the vibrational and rotational modes appear to be equilibrated, the vibrational and rotational temperatures determined by Zube and Myers from N_2 show very different trends than did NH in this work [7]. As seen in Figure 8, the N_2 temperatures exhibited a significant decline during the expansion. The peak rotational and vibrational temperatures varied from about 8,000 K at an area ratio of approximately 15 to 2,400 K at an area ratio of 125. This was very different from the NH vibrational and rotational temperatures determined in this work which exhibited a nearly constant temperature in the neighborhood of 4,000 K. The differing behavior of these two cases is possibly due to the different propellant chemistries. The nonuniform properties of the plasma within the arcjet expansion may result in N_2 and NH existing in different portions of the flow. Or more likely, the chemical kinetics responsible for the formation of each species may influence the temperatures observed. In the case of Zube and Myers, the simulated hydrazine propellant consisted of 33% N_2 which obviously did not require it to be formed from either dissociation or recombination processes. Therefore, N_2 and NH arose from very different mechanisms in these two tests and comparisons between the two species are likely to be misleading.

Electron Densities

The hydrogen Balmer beta transition showed increased broadening in the upstream direction of the nozzle indicative of increasing electron density and thermal temperature. Figure 9 shows the Balmer beta line shape at all four locations it was sampled. The line shape observed at the exit plane is the narrowest with the widest line profile observed at the first optical port.

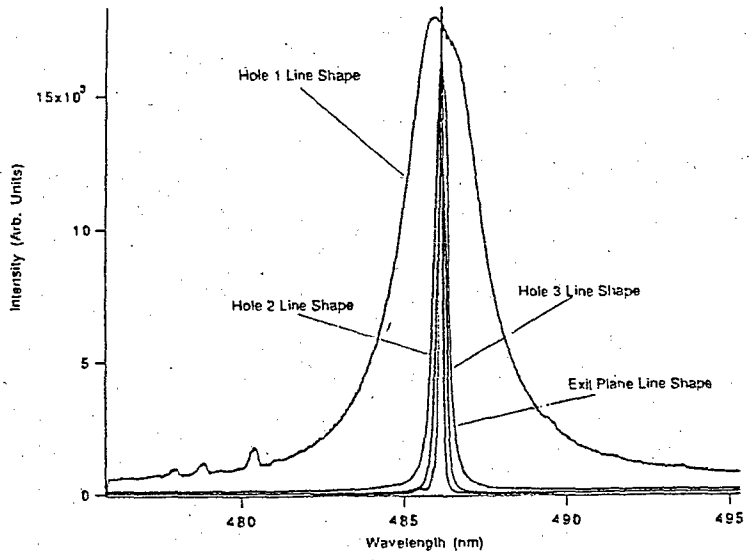

Figure 9. Balmer Beta Profiles

The FWHM of the Balmer beta transition was used to determine the electron density using Equation 3 and the data tabulated by Griem [11]. In each case, the electron temperature was assumed to be equal to the local hydrogen excitation temperature which is thought to best represent the average electron temperature across the nozzle. For port 1, an electron temperature of 8,500 K is used and the electron density is computed to be 3.28×10^{15} cm^{-3}. For port 2, the electron temperature is 4,800 K and the electron density is determined to be 1.03×10^{15} cm^{-3}. For port 3, an electron density of 8.44×10^{14} cm^{-3} was found. Finally, the electron density at the exit plane is 4.02×10^{14} cm^{-3}. The results for all four locations are presented in Figure 10.

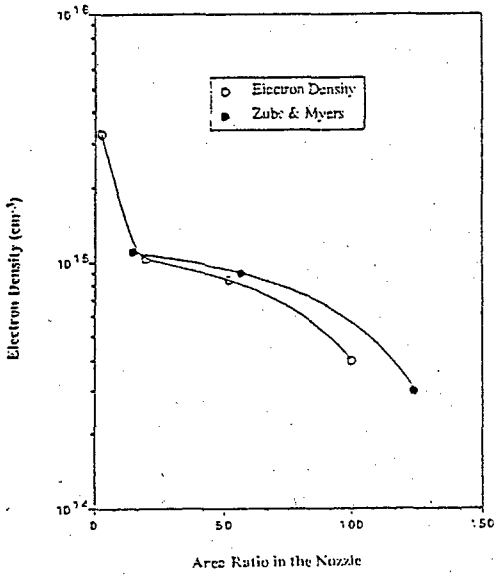

Figure 10. Electron Densities

As shown in Figure 10, a sudden change in the electron density is apparent between access holes 1 and 2 with a steady decline after hole 2 until the nozzle exit plane. This initial drop in the electron density within the expansion nozzle may most likely be attributed to arc attachment. Downstream of hole 1, it is believed that the arc diffuses as it attaches to the nozzle/anode wall. Upstream of the arc attachment, electron densities would be significantly higher due to the continuous ionization of plasma species within the core flow from collisional Joule heating of the propellant. Whereas, downstream of the attachment point, the arc is no longer available to replenish the free electrons lost due to recombination, and the electron density subsequently falls. Therefore, it is postulated that the arc attachment point might lie between ports 1 and 2.

During the calculation of the electron densities, the Doppler, or thermal, broadening component of the line widths were calculated using the following expression,

$$\Delta\lambda_D = \lambda\sqrt{\frac{2kT_{Tran}}{Mc^2}} \qquad (4)$$

where $\Delta\lambda_D$ is the Doppler component of the FWHM of the transition, M is the mass of the emitting species, T_{Tran} is the translational temperature of the emitting species, and λ is the wave length of the transition [11]. The Voigt profiles tabulated by Wiese were then used to determine the fraction of broadening due to each mechanism [20]. The line shape observed in port one was found to be less than 1% influenced by Doppler broadening. The data most influenced by Doppler broadening was the line shape from the exit plane which showed an influence of less than of 4% of the FWHM. Following the approach of Wiese, these lines were deemed to be dominated by Stark broadening and electron density calculations were made from the FWHM observed without a need for deconvolution of the line profile.

If PLTE is assumed to dominate when the collisional rate is 10 times the radiative decay rate, the following expression gives the electron density and principle quantum number above which PLTE is valid.

$$n_e \geq 7 \times 10^{18} \frac{z^7}{n^{17/2}} \left(\frac{kT_e}{z^2 E_H} \right)^{1/2} \qquad (5)$$

where n_e is the electron density in cm^{-3}, z is the ionic charge, n is the principle quantum level, and E_H is the ionization potential of the hydrogen atom [11]. The requisite principle quantum number for hydrogen at which PLTE is defined varied from 2.2 at the first port to 2.7 at the exit plane. This behavior was corroborated by the Boltzmann plots. At port 1, the first transition was deemed to be out of equilibrium and discarded. However, the remaining three transitions were sufficient to produce an excitation temperature. At the exit plane, the first 3 transitions of the Balmer series were deemed to be underpopulated by the lack of linearity with the upper transitions and were thus also discarded. The electron densities therefore appear to be consistent with the electron temperatures and measures of non-equilibrium determined from the hydrogen Boltzmann plots at the optical access points.

The interior electron densities found in this work were very similar to those previously reported for a 1 kW arcjet [7]. This was not initially expected due to the higher specific powers in this test (71 versus 25 MJ/kg). The decline of electron density in the downstream portion of the expansion is nearly identical to that measured for a low power arcjet. However, this work showed a very different electron density at the first hole which was at a smaller nozzle area ratio than any of the previously reported data points. It appears that a major change in the mechanisms governing the electron density occurs between holes 1 and 2, likely indicating arc attachment in this region.

Conclusions

Emission spectroscopy of the interior plasma of a radiatively cooled, high power arcjet is a viable diagnostic for the observation of interior plasma energy modes. It is believed that the placement of optical access ports through the anode did

not significantly perturb the arcjet. Future tests with a thrust stand will be utilized to determine the validity of this assumption.

Most of the same plasma diagnostic techniques can be adapted to the investigation of the arcjet interior with minimal difficulty even though like a low power arcjet, the plasma within a high power model is strongly non-equilibrium. For the high power case, excitation temperatures within the arcjet nozzle are readily found from hydrogen and NII. In addition, the hydrogen Balmer beta transition provides a convenient method to determine the electron density within the arcjet plasma. Analysis indicates that the line shape of the beta Balmer line is at least 95% dominated by Stark broadening from near the constrictor exit to the exit plane of the nozzle.

The molecule NH was found to exist throughout the expansion nozzle. Due to the apparent lack of NI within the nozzle, NH is thought to be primarily an ammonia dissociation product that is formed within the constrictor and plenum chamber rather than a recombination product in the arcjet nozzle boundary layer. Vibrational and rotational temperatures of NH were readily determined. The NH vibrational and rotational energy modes appear to be frozen and in equilibrium with each other throughout the arcjet nozzle expansion. It is not known whether this behavior is due to flow nonuniformities that concentrate the NH population along the nearly constant temperature anode wall, or due to nonequilibrium effects affecting the measurements. The lack of NI in evidence within the arcjet was deemed to be due to the differences in chemical kinetics caused by a lack of molecular nitrogen in the propellant as was used by previous researchers. Some evidence of nonequilibrium was seen in the experimental data where the rotational structure of the band exhibited a non-Boltzmann population distribution among the rotational levels. However, this behavior was not excessive and there is a significant degree of confidence in the rotational temperature measurements. Strong evidence exists that the vibrational temperature as determined is skewed by nonequilibrium populations within the vibrational levels of NH.

Hydrogen excitation temperatures were found to be significantly lower in this work than for a 1 kW arcjet [7]. This was not completely understood. Since nonequilibrium effects were seen to severely underpopulate the alpha and beta transitions, it is believed that the plasma conditions within an arcjet require that temperatures be determined by more than 2 transitions as was done in reference 7. The nonuniformities of the propellant flow within the nozzle are also thought to result in the NII and hydrogen species exhibiting differing excitation temperatures due to their relative populations in different regions of the flow. There are many issues that still must be resolved in the arcjet interior. Further studies at different power levels and propellant would result in an increased understanding of the plasma dynamics of the arcjet expansion process. However, in order to resolve the outstanding issues with respect to the unexpected low temperatures for this high power thruster, complete internal radial profiles must be taken with proper Abel inversion.

Acknowledgments

This work was supported by AFSOR Task 2308M4 and the Air Force Palace Knight Program. The authors also wish to thank Rich Welle of Aerospace Corporation for providing the NH spectral code.

References

1. Smith, W.W., et al., "Low Power Hydrazine Arcjet Qualification," Paper IEPC 91-148, 22nd International Electric Propulsion Conference, Viareggio, Italy, Oct. 1991.
2. Sutton, A.M. "Overview of the Air Force ESEX Flight Experiment," Paper IEPC 93-057, 23rd International Electric Propulsion Conference, 13-16 Sept. 1993, Seattle, WA.
3. Tahara, H., T. Sakakibara, K. Onoe, and T. Yoshikawa, "Experimental and Numerical Studies of a 10 kW Water-Cooled Arcjet Thruster," Paper IEPC 91-015, 22nd International Electric Propulsion Conference, 14-17 Oct. 1991, Viareggio, Italy.
4. Tahara, H., N. Uda, K. Onoe, and Y Tsubakishita, "Optical Measurement and Numerical Analysis of Medium Power Arcjet Non-Equilibrium Flowfields," Paper IEPC 93-133, 23rd International Electric Propulsion Conference, 13-16 Sept., 1993, Seattle, WA.
5. Storm, P.V. and M.A. Cappelli, "Axial Emission Diagnostics of a Low Power Hydrogen Arcjet Thruster," Paper IEPC 93-219, 23rd International Electric Propulsion Conference, 13-16 Sept. 1993, Seattle, WA.
6. Ruyten, W.M., D. Burtner, and D. Keefer, "Spectroscopic Investigation of a Low-Power Arcjet Plume," Paper AIAA 93-1790, 29th Joint Propulsion Conference, 28-30 June 1993, Monterey, CA.
7. Zube, D.M. and R.M. Myers, "Nonequilibrium in a Low Power Arcjet Nozzle," Paper AIAA 91-2113, 27th Joint Propulsion Conference, 24-27 June 1991, Sacramento, CA.
8. Zube, D.M. and M. Auweter-Kurtz, "Spectroscopic Arcjet Diagnostic Under Thermal Equilibrium and Non-Equilibrium Conditions," Paper AIAA 93-1792, 29th Joint Propulsion Conference, 28-30 June, 1993, Monterey, CA.
9. Deininger, W.D., A. Chopra, T.J. Pivirotto, K.D. Goodfellow, and J.W. Barnett, "30 kW Ammonia Arcjet Technology: Final Report July 1986-December 1989." JPL Publication 90-4, 15 Feb. 1990.
10. Boulos, M., P. Fauchais, and E. Pfender, *Diagnostic Techniques in Thermal Plasma Processing*, U.S. Department of Energy, February 1986.
11. Griem, Hans R., *Plasma Spectroscopy*, McGraw-Hill Book Company, New York, 1964.
12. Pearse, R.W.B. and A.G. Gaydon, *The Identification of Molecular Spectra*, John Wiley and Sons, Inc, New York, 1976.
13. Dixon, R.N., "The 0-0 and 1-0 Bands of the $A^3\Pi \rightarrow X^3\Sigma^-$ System of NH," *Canadian Journal of Physics*, Vol. 37, p. 1171, 1959.
15. Herzberg, Gerhard, *Molecular Spectra and Molecular Structure: Volume I - Spectra of Diatomic Molecules*, Krieger Publishing Company, Malabar, FL, 1989.

16. Croften, M.W., R.P. Welle, S.W. Janson, and R.B. Cohen, "Rotational and Vibrational Temperatures in the Plume of a 1-kW Ammonia Arcjet," Paper AIAA 91-1491, AIAA 22nd Fluid Dynamics , Plasma Dynamics & Lasers Conference, June 24-26, 1991, Honolulu, HI.
17. Welle, R.P., Personal Communication, Los Angeles, CA, February 1994.
18. Jahn, R.G., *Physics of Electric Propulsion*, McGraw-Hill Book Co., New York, 1968.
19. Bennet, R.G. and F.W. Dalby, "Experimental Oscillator Strengths of CH and NH," *The Journal of Chemical Physics*, Vol. 32, No. 6, 1960.
20. Wiese, W.L., "Line Broadening," *Plasma Diagnostic Techniques*, Eds. Richard H. Huddlestone and Stanley L. Leonard, Academic Press, New York, 1965.
21. Weast, Robert C., Editor, *Handbook of Chemistry and Physics*, CRC Press, Inc., Boca Raton, FL, 69th edition, 1988.